Thermodynamic Stability of $LaMnO_3$ and its competing oxides: A Hybrid Density Functional Study of an Alkaline Fuel Cell Catalyst

E. A. Ahmad[1,2], L. Liborio[1,2], D. Kramer[1,3], G. Mallia[1,2], A. R. Kucernak[1] and N. M. Harrison[1,2,4*]

[1] *Department of Chemistry, Imperial College London, South Kensington, London SW7 2AZ, UK*

[2] *Thomas Young Centre, Imperial College London, South Kensington, London SW7 2AZ, UK*

[3] *Faculty of Engineering and the Environment , University of Southampton, University Road, Southampton SO17 1BJ, UK*

[4] *Daresbury Laboratory, Daresbury, Warrington, WA4 4AD, UK*

(Dated: April 13, 2011)

Abstract

The phase stability of $LaMnO_3$ with respect to its competing oxides is studied using hybrid-exchange density functional theory (DFT) as implemented in CRYSTAL09. The underpinning DFT total energy calculations are embedded in a thermodynamic framework that takes optimal advantage of error cancellation within DFT. It has been been found that by using the *ab initio* thermodynamic techniques described here, the standard Gibbs formation energies can be calculated to a significantly greater accuracy than was previously reported (a mean error of 1.6% with a maximum individual error of -3.0%). This is attributed to both the methodology for isolating the chemical potentials of the reference states, as well as the use of the B3LYP functional to thoroughly investigate the ground state energetics of the competing oxides.

PACS numbers:

*Electronic address: ehsan.ahmad08@imperial.ac.uk

I. INTRODUCTION

$LaMnO_3$ is well known as a perovskite material that can exhibit useful properties for magnetic sensors and solid oxide fuel cells (SOFCs)[1–3]. A recent study has also revealed promising catalytic activity for $LaMnO_3$ to facilitate oxygen reduction in alkaline fuel cells (AFCs) [4]. This presents a great opportunity for commercialisation of AFC technology, since $LaMnO_3$ has a significant economic advantage over noble metals.

AFCs differ greatly with respect to SOFCs, as they use a liquid electrolyte, usually KOH, and therefore operate in a significantly lower temperature range (25-70°C) [5]. This introduces a completely different environment, where the materials used for the catalysis of oxygen reduction on the cathode are expected to behave differently. $LaMnO_3$ has to be studied under these conditions to understand its bulk properties and corresponding surfaces. For this purpose, a complete picture of the thermodynamic stability of $LaMnO_3$ with respect to the competing oxides (La_2O_3, MnO_2, Mn_2O_3, Mn_3O_4 and MnO) is necessary.

$LaMnO_3$ has been studied extensively by experiment (with X-ray [6–11] and neutron diffraction [7, 12], scanning [10, 11] and transmission electron microscopy [10], electron paramagnetic resonance [9], thermogravimetry (TG) [6, 10, 12, 13], differential thermal analysis (DTA) [11, 12], differential scanning [6, 8, 10] and alternating current calorimetry [8]). However, not much literature can be found that investigates the factors affecting the reactivity of $LaMnO_3$ as a catalyst in an AFC environment [14]. This is also true from a theoretical point of view, and although the electronic structure of the low temperature orthorhombic phase of $LaMnO_3$ is well understood (by adopting unrestricted Hartree-Fock [15, 16] and hybrid-exchange density functional theory [17, 18]), there is a lack of knowledge of surface properties. Instead, the majority of such studies were directed towards understanding the surface of the high temperature cubic phase, with relevance to SOFC conditions [19–23]. Efforts to understand the thermodynamics and surface properties of orthorhombic $LaMnO_3$ can be found in recent literature [24, 25], but there has been no comprehensive study of the thermodynamics of orthorhombic $LaMnO_3$ and its competing oxides.

Concerning the series of manganese oxides, there is a large number of papers which explore their properties, including efforts directly related to the thermodynamics. The heat capacity has been obtained by calorimetry, and the thermal stability and phase transitions have been analysed by TG, differential TG and DTA [26–29]. Quantum mechanical sim-

FIG. 1: The crystallographic cell for $LaMnO_3$ and the competing oxides in the geometries indicated in Table II. Large, medium and small spheres correspond to the La, O and Mn atoms. In the case of MnO_2 and Mn_3O_4, the labelling of the Mn atoms is linked to the assignment of spin in tables II and III. Symmetry irreducible Mn atoms are given in gray scale color for Mn_2O_3 for clarity.

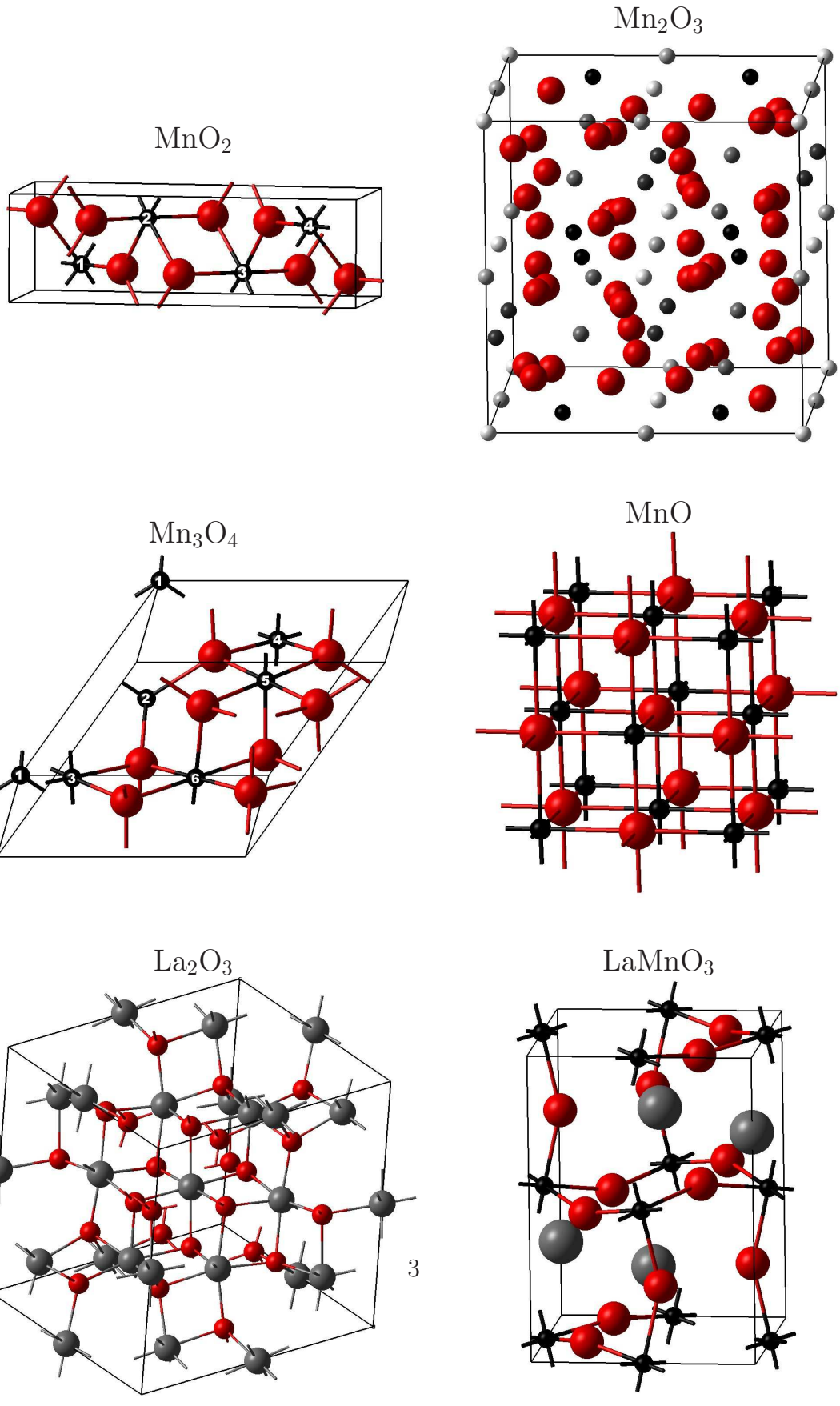

ulations have been performed to study the formation energies of this series by adopting different density functionals (PW91 [25] and, PBE, PBE+U, PBE0 and HSE [30]). The energetics of these compounds are characterized by a strong interplay between geometry and electronic structure, thus requiring an accurate treatment of exchange and correlation for the description of the electron localization. This is especially important to get a consistent set of formation energies, as Mn adopts different valence states within the series. Previously calculated formation energies are affected by a significant error relative to experiment, – the mean error is in the range of 7-17% [25, 30]. Apart from the inaccuracy of GGA-type functionals regarding the energetics of correlated systems, this can also be attributed to the methodology adopted to calculate the chemical potential of Mn and O, as pointed out in Section IV B.

A proper estimation of the formation energies of the various competing compounds is crucial to build the phase diagram. Even small energetic inaccuracies ($\sim$7%) paint a completely different picture of phase stability in the La-Mn-O system, as demonstrated in Section IV C. Therefore, it is worth pointing out that no previous study has been able to provide an accurate representation of the stability regions of $LaMnO_3$ with respect to all of the competing oxides.

The aim of this study is to calculate the bulk phase diagram of the La-Mn-O system and to outline a suitable methodology for the study of the thermodynamics of the compounds in this multivalent series. In addition, an investigation of the ground state of the compounds with regards to their geometry and magnetic state is performed. The hybrid exchange density functional B3LYP has been adopted, since it is well documented that it provides an accurate description of the electronic structure of localised and correlated systems [31, 32]. The paper is organised as follows: in Section II the methodology is outlined; in Section III the computational details are provided; in Section IV the results are discussed, and conclusions are drawn in Section V.

II. METHODOLOGY

In this section, the methodology used to construct the phase diagram is described. This relies on the calculation of the Gibbs formation energies, ΔG_f^0, of all of the compounds of involved. This in turn requires the determination of the standard chemical potentials of the

elements, μ^0.

We will generally neglect entropic and volumetric work contributions to the Gibbs energy and approximate G with the total energy E at 0 K as given by DFT. This is well justified for solids in the temperature and pressure range of interest, because the entropic contribution is mainly vibrational and the volume of solids is nearly independent of pressure and temperature. Hence, these terms are small and tend to cancel [33]. The reference state for oxygen, however, is the gaseous dimer and needs further consideration. The Gibbs energy of an (ideal) gas contains significant translational and rotational entropy as well as volumetric work.

The following expression for the oxygen chemical potential as a function of of p_{O_2} and T reflects this [34]:

$$\mu_{O_2}(p_{O_2}, T) = E_0 + (\mu^0_{O_2} - E_0)\frac{T}{T^0} - \frac{5k_B}{2}T\ln\left(\frac{T}{T^0}\right) + k_B T \ln\left(\frac{p_{O_2}}{p^0_{O_2}}\right) \quad (1)$$

This expression contains two unkown quantities: E_0, the energy per O_2 molecule at 0K and $\mu^0_{O_2}$, the chemical potential of an O_2 molecule at standard conditions (where superscript 0 indicates standard conditions: $T^0 = 298.15$K and $p^0_{O_2} = 1$bar). E_0 is easily calculated using the B3LYP functional with DFT as outlined in Section III, while $\mu^0_{O_2}$ is normally estimated using experimental data. Since we need $\mu^0_{O_2}$, rather than $\mu_{O_2}(p_{O_2}, T)$ to calculate the Gibbs formation energies, it is useful to adapt this expression for this purpose. To do so, it is neccesary to introduce the the Shomate equation, which expresses the temperature dependence of the Gibbs free energies per mole at standard pressure, at $p_{O_2} = p^0_{O_2}$:

$$\mu^0_{O_2}(t) = \mu^0_{O_2} + t^0 S^0 + A(t - t\ln(t)) - B\frac{t^2}{2} - C\frac{t^3}{6} - D\frac{t^4}{12} - E\frac{1}{2t} + F - Gt - H \quad (2)$$

where t = T/1000 and the coefficients given in table I. By equating the temperature derivatives of Equations 1 and 2 at $p_{O_2} = p^0_{O_2}$, $\mu^0_{O_2}(T)$ is obtained:

$$\mu^0_{O_2}(T) = E_0 + T^0\left[\frac{5k_B}{2}\ln\left(\frac{T}{T^0}\right) + \frac{5k_B}{2} + \frac{1}{1000}\left[-A\ln(t) - Bt - \frac{1}{2}Ct^2 - \frac{1}{3}Dt^3 + \frac{E}{2t^2} - G\right]\right] \quad (3)$$

which relies on only one unkown quantity E_0 and gives us $\mu^0_{O_2}$ when $T = T^0$.

Instead of relying on DFT to provide energetics for the metallic reference states of La and Mn, we adopt an approach where the chemical potential of La and Mn in their standard

TABLE I: The parameters for the range 100 - 700 K [35].

A	31.32234× 10^3 kJ/(mol K)
B	-20.23531× 10^6 kJ/(mol K^2)
C	57.86644× 10^9 kJ/(mol K^3)
D	-36.50624× 10^{12} kJ/(mol K^4)
E	-0.007374× 10^{-3} kJ K/mol
F	-8.903471 kJ/mol
G	246.7945 kJ/mol
H	0 kJ/mol

states is obtained using the Gibbs formation energy of their oxides. This avoids the need to compare DFT energies for oxides and metals which is likely to introduce significant error due to the lack of error cancellation. The general formula for the formation energies of these oxides is:

$$\Delta G^0_{f\mathrm{M_xO_y}} = \mu^{bulk}_{\mathrm{M_xO_y}} - x\mu^0_{\mathrm{M}} - y\mu^0_{\mathrm{O}} \tag{4}$$

where M and O are metal and oxygen in the oxide $\mathrm{M_xO_y}$, $\Delta G^0_{f\mathrm{M_xO_y}}$ is the standard Gibbs formation energy from experiment [36] and $\mu^{bulk}_{\mathrm{M_xO_y}}$ is the chemical potential (Gibbs energy) of the bulk oxide. In the case of La, μ^0_{La} is calculated from the following equation for $\mathrm{La_2O_3}$ by introducing the value of $\mu^0_{\mathrm{O_2}}$ given by the previous method.

$$\Delta G^0_{f\mathrm{La_2O_3}} = \mu^{bulk}_{\mathrm{La_2O_3}} - 2\mu^0_{\mathrm{La}} - \frac{3}{2}\mu^0_{\mathrm{O_2}} \tag{5}$$

where the potential for the bulk $\mathrm{La_2O_3}$, $\mu^{bulk}_{\mathrm{La_2O_3}}$, can be equated to the ground state energy, as discussed earlier [33]. In the case of the manganese oxides the same approach can be applied; however, since there are several oxides, slightly different manganese chemical potentials arise. These values have to be averaged to provide a value to calculate the *ab initio* formation energies of the manganese oxides and $\mathrm{LaMnO_3}$. The quantities, μ^0_{La}, μ^0_{Mn} and $\mu^0_{\mathrm{O_2}}$, define the upper stability limits in terms of the chemical potentials μ_{La}, μ_{Mn} and $\mu_{\mathrm{O_2}}$ for any compound in the system. Therefore it is true that:

$$\mu_i - \mu^0_i \leq 0 \tag{6}$$

where $i = \mathrm{La, Mn, O}$. Above these limits the compounds decompose into their constituent elements. These conditions can be used to introduce a change of variable, $\Delta\mu_i = \mu_i - \mu^0_i$ to

give:

$$\Delta\mu_i \leq 0 \tag{7}$$

which is convenient for the construction of a phase diagram. For example, the equilibrium chemical potential of $LaMnO_3$ with respect to its elements, given by:

$$\mu_{\mathrm{La}} + \mu_{\mathrm{Mn}} + \frac{3}{2}\mu_{\mathrm{O_2}} = \mu^{bulk}_{\mathrm{LaMnO_3}} \quad , \tag{8}$$

can be expressed as:

$$\Delta\mu_{\mathrm{La}} + \Delta\mu_{\mathrm{Mn}} + \frac{3}{2}\Delta\mu_{\mathrm{O_2}} = \Delta G^0_{f\mathrm{LaMnO_3}} \tag{9}$$

by stoichiometrically subtracting μ^0_{La}, μ^0_{Mn} and $\mu^0_{\mathrm{O_2}}$ from both sides of Equation 8. Note that the stoichiometrically weighted chemical potentials $\Delta\mu^0_{\mathrm{La}}$, $\Delta\mu^0_{\mathrm{Mn}}$ and $\Delta\mu^0_{\mathrm{O_2}}$ must sum to $\Delta G^0_{f\mathrm{LaMnO_3}}$. Hence, as has been pointed out [37], $\Delta\mu_i$ for each element is not allowed to become so negative (i.e. more negative than $\Delta G^0_{f\mathrm{LaMnO_3}}$) that the others break their upper limit $\Delta\mu_i \leq 0$. Therefore, in the case of $LaMnO_3$, the lower limits for the chemical potentials μ_i are defined as:

$$\Delta\mu_i \geq \frac{1}{x_i}\Delta G^0_{f\mathrm{LaMnO_3}} \tag{10}$$

with x_i equal to the stoichiometric coefficient of i. When combining Equations 7 and 10, it follows that

$$\frac{1}{x_i}\Delta G^0_{f\mathrm{LaMnO_3}} \leq \Delta\mu_i \leq 0 \tag{11}$$

By considering Equation 9 and the limits that have been discussed, a region in the La-Mn-O chemical potential space can now be defined where $LaMnO_3$ is stable with respect to the reference states. The competing phases, however, impose similar conditions and further limit the range of chemical potentials which stabilise $LaMnO_3$. Accordingly, a phase diagram can be constructed to show the stability region for $LaMnO_3$ by considering the equivalent equations for each of the competing oxides.

III. COMPUTATIONAL DETAILS

All calculations have been performed using the CRYSTAL09 [38] software package, based on the expansion of the crystalline orbitals as a linear combination of a local basis set (BS) consisting of atom centred Gaussian orbitals. The Mn and O atoms are described by a triple valence all-electron BS: an 86-411d(41) contraction (one s, four sp, and two d shells) and

an 8-411d(1) contraction (one s, three sp, and one d shells), respectively; the most diffuse sp(d) exponents are α^{Mn}=0.4986(0.249) and α^{O}= 0.1843(0.6) Borh^{-2} [39]. The La basis set includes a nonrelativistic pseudopotential to describe the core electrons, while the valence part consists of a 411p(411)d(311) contraction scheme (with three s, three p and three d shells); the most diffuse exponent is α^{La}=0.15 Borh^{-2} for each s,p and d [17].

Electron exchange and correlation are approximated using the B3LYP hybrid exchange functional, which, as noted above, is expected to be more reliable than LDA or GGA approaches [31, 32]. The exchange and correlation potentials and energy functional are integrated numerically on an atom centred grid of points. The integration over radial and angular coordinates is performed using Gauss-Legendre and Lebedev schemes, respectively. A pruned grid consisting of 99 radial points and 5 sub-intervals with (146, 302, 590, 1454, 590) angular points has been used for all calculations (the XXLGRID option implemented in CRYSTAL09 [38]). This grid converges the integrated charge density to an accuracy of about $\times 10^{-6}$ electrons per unit cell. The Coulomb and exchange series are summed directly and truncated using overlap criteria with thresholds of 10^{-7}, 10^{-7}, 10^{-7}, 10^{-7} and 10^{-14} as described previously [38, 40]. Reciprocal space sampling was performed on a Pack-Monkhorst net with a shrinking factor comparable to IS=8 for the smallest cell of MnO. The self consistent field procedure was converged up to a tolerance in the total energy of $\Delta E = 1 \cdot 10^{-7} E_h$ per unit cell.

The cell parameters and the internal coordinates have been determined by minimization of the total energy within an iterative procedure based on the total energy gradient calculated analytically with respect to the cell parameters and nuclear coordinates. Convergence was determined from the root-mean-square (rms) and the absolute value of the largest component of the forces. The thresholds for the maximum and the rms forces (the maximum and the rms atomic displacements) have been set to 0.00045 and 0.00030 (0.00180 and 0.0012) in atomic units. Geometry optimization was terminated when all four conditions were satised simultaneously.

IV. RESULTS

A. Geometries and Energetics

The optimized lattice parameters of the most stable (crystallographic/magnetic) phases for $LaMnO_3$ and the competing oxides are given in Table II. For the competing oxides some of the other commonly observed crystallagrapic phases and magnetic configurations have been investigated and the results are reported in Table III. The ΔE is the increase in energy from the most stable phase and magnetic configuration of the corresponding compound given in Table II.

Only the low temperature phase of $LaMnO_3$, which is orthorhombic and A-type antiferromagnetic (AAF) [18, 41, 52], has been simulated. The calculated lattice parameters **b** and **c** are in good agreement with the experimental values; the percentage error is less than 1.5%. The **a** parameter, however, is overestimated by almost 5% with respect to the low temperature (9K) structure cited. It is noted that there is no experimental certainty for this parameter; values between 5.472-5.748 Å are reported[42]. Only two sets of values based on theory have been reported previously. In one case, the unrestricted Hartree-Fock level of theory is used ($a = 5.740$ $b = 7.754$ $c = 5.620$ [16]), while in the other the generalized gradient approximation (GGA) to DFT is adopted ($a = 5.7531$ $b = 7.7214$ $c = 5.5587$ [24]); both predict a value of a close to the upper limit observed experimentally.

The only competing binary oxide containing La is La_2O_3, which occurs in a body-centered cubic structure for the most stable phase (see Table II) and in the trigonal structure at high temperature (see Table III) [42, 44, 53]. Both are non-magnetic.

The competing binary Mn oxides are discussed in terms of oxidation state as follows: MnO_2(IV), Mn_2O_3(III), Mn_3O_4(II/III) and MnO(II). For the manganese oxides in Table II the percentage error between the experimental and calculated lattice parameters is less than 2.3% [32].

The lowest energy for MnO_2 was found for the orthorhombic (ramsdellite) antiferromagnetic (AFM) structure, with the spin configuration as indicated by the arrows in Table II. The differences in energy between various spin configurations both within and in between the orthorhombic and rutile (pyrolusite) structures, are of the order of tens of meV. This can be linked to the high number of polymorphs observed for this material [54, 55]. This finding is

TABLE II: Experimental and optimized lattice parameters (**a**, **b** and **c** in Å) of the most stable (crystallographic/magnetic) phases at low temperature for $LaMnO_3$ and the competing oxides. The magnetic solution is indicated in the second column as AFM, FM and NM for the antiferromagnetic, ferromagentic and non-magnetic case; the type of AFM is labelled by (A) and (G), see Ref. [41]. The arrows proceeding the type of magnetic phase indicate the spin direction of the sequence of Mn atoms in the cell according to Figure 1. The temperature at which the experimental geometry was obtained is given in the column labelled T(K) accoding to Ref. [42]; a specified range indicates where the compound is stable. The percentage error (%) of the calculated lattice parameters relative to the experimental parameters cited for the compound, are also included in italics.

Compound			Space Group	**a**	**b**	**c**	T(K)	Ref.
$LaMnO_3$		Exp.	Pnma (62)	5.730	7.672	5.536	9	[43]
	AFM (A)	Opt.		6.010	7.735	5.614		
				4.89	*0.82*	*1.41*		
La_2O_3		Exp.	Ia3 (206)	11.360	-	-	≤770	[44]
	NM	Opt.		11.583	-	-		
				1.96	-	-		
MnO_2		Exp	Pnma (62)	9.273	2.864	4.522	298	[45]
	AFM ↑↓↑↓	Opt.		9.269	2.882	4.624		
				-0.04	*0.62*	*2.26*		
Mn_2O_3		Exp.	Pbca (61)	9.416	9.423	9.405	≤302	[46]
	FM	Opt.		9.479	9.538	9.566		
				0.67	*1.22*	*1.71*		
Mn_3O_4		Exp.	I41/amd (141)	5.757	-	9.424	10	[47]
	FiM ↑↑↓↓↑↑	Opt.		5.814	-	9.558		
				0.99	-	*1.42*		
MnO		Exp.	Fm3m (225)	4.444	-	-	293	[48]
	AFM (G)	Opt.		4.458	-	-		
				0.32	-	-		

in agreement with previous work, but it has to be noted that the stability order is reverted,

TABLE III: Experimental and optimised lattice parameters of some of the other commonly observed structures. Annotation is the same as table II, with the addition of **ΔE (meV)**, which is the increase in energy from the most stable geometry and magnetic configuration of the corresponding compound given in Table II. * indicates temperature at which the sample was synthesised

Compound			Space Group	**a**	**b**	**c**	ΔE	T(K)	Ref.
La_2O_3		Exp.	P$\bar{3}$m1 (164)	3.937	-	6.129		≥770	[44]
	NM	Opt.		3.999	-	6.331	**136**		
MnO_2		Exp	Pnma (62)	9.273	2.864	4.522		298	[45]
	FM	Opt.		9.199	2.885	4.674	**43**		
	AFM ↑↓↓↑	Opt.		9.264	2.880	4.627	**8**		
	AFM ↓↓↑↑	Opt.		9.202	2.886	4.677	**39**		
		Exp	P42/mnm (136)	4.404	-	2.877			[49]
	FM	Opt.		4.441	-	2.895	**67**		
	AFM	Opt.		4.429	-	2.894	**31**		
Mn_2O_3		Exp.	Ia3 (206)	9.417	-	-		723	[50]
	FM	Opt		9.520	-	-	**249**		
Mn_3O_4		Exp.	I41/amd (141)	5.757	-	9.424		10	[47]
	FM	Opt.		5.842	-	9.560	**200**		
	FiM ↑↑↓↓↓↓	Opt.		5.800	-	9.577	**12**		
	FiM ↑↓↑↑↑↑	Opt.		5.822	-	9.554	**99**		
	FiM ↑↑↑↓↑↓	Opt.		5.809	5.825	9.566	**94**		
	FiM ↑↑↑↓↑↑	Opt.		5.821	5.832	9.558	**100**		
	FiM ↑↓↑↓↑↓	Opt.		5.818	-	9.554	**82**		
		Exp.	Pbcm (57)	3.026	9.769	9.568		1000*	[51]
	FM	Opt.		3.069	9.977	9.637	**770**		
MnO		Exp.	Fm3m (225)	4.444	-	-		293	[48]
	FM	Opt.		4.483	-	-	**96**		

when paramagnetic energies are obtained by fitting a Heisenberg Hamiltonian [55]. In fact, the rutile structure is reported to have a lower energy (by 22 meV) with respect to the

orthorhombic one [55].

Mn_2O_3 was simulated in its cubic and orthorhombic forms. The relative energies agree with experiment, where the orthorhombic structure is considered stable at low temperature [46, 50]. The structure was only simulated in its ferromagnetic (FM) form as there is no consensus yet on its low temperature magnetic structure from experiment [56, 57].

Although Mn_3O_4 has a non-collinear magnetic structure with long range ordering [58, 59], the simulation has been limited to ferromagnetic and ferrimagnetic (FiM) configurations that can be defined within the primitive cell, consistent with previous work [30]. The spinel FiM $\uparrow\uparrow\downarrow\downarrow\uparrow\uparrow$ configuration (see Figure 1 for notation) is the most stable. In Table III the various FiM/FM configurations of the spinel Mn_3O_4 are shown, differing within a range of 200 meV, while the high-pressure orthorhombic phase is drastically less stable (ΔE =770 meV).

MnO has a faced-centered cubic G-type antiferromagnetic structure at low temperature (T_N=118K); the spins order ferromagnetically on (111) planes with antiferromagnetic coupling between neighbouring planes [60, 61]. The optimised structure is characterized by a uniform distortion of the cell angles by 1.52% indicating that at low temperatures the unit cell of MnO becomes rhombohedrally distorted, in agreement with Hartree-Fock calculations [62] and neutron diffraction studies [61]. In addition, the distance between antiferromagnetically coupled Mn is shorter (3.135Å) compared to the ferromagnetically coupled Mn (3.170Å); therefore, a contraction occurs normal to the ferromagnetic (111) planes corresponding to a magnetostriction effect. This does not occur in the FM phase, which has an energy 96meV higher and an Mn-Mn distance of 3.170Å.

B. Gibbs formation energies

The calculated Gibbs formation energies for the stable (lowest energy) phases of $LaMnO_3$ and the competing Mn oxides are compared in Table IV with experimental Gibbs formation energies obtained from a thermochemical database [36]. For La_2O_3, the calculated and experimental $\Delta_f G$ are identical by construction (cf. Section II), therefore it is omitted from this table.

The maximum percentage error of $\Delta_f G^0$ relative to the experimental value in Table IV does not exceed $\pm 3\%$; a positive (negative) error means that the Gibbs formation energy

TABLE IV: Gibbs free energy of formation (eV) for $LaMnO_3$ and the manganese oxides [36, 64].

Compound	**Experimental** $\Delta_f G^0$	**Calculated** $\Delta_f G^0$	**Error**(%)
$LaMnO_3$	-14.03	-13.89	*-1.0*
MnO_2	-4.82	-4.68	*-3.0*
Mn_2O_3	-9.13	-9.21	*0.9*
Mn_3O_4	-13.30	-13.61	*2.4*
MnO	-3.76	-3.76	*<0.1*

is underestimated (overestimated). The mean relative error is 1.6%. The atypical large error for MnO_2 is noteworthy. It can be attributed to the natural occurance of Ruetschi defects in ramsdellite (orthorhombic MnO_2) [55]; this can stabilise the experimental energies with respect to the (defect free) calculated energy, because low energy defects introduce configurational entropy and lower the Gibbs enery.

In general, the calculated formation energies of the manganese oxides are in very good agreement with experiment. This highlights the quality of the hybrid-exchange functional B3LYP, which is able to consistently describe the oxygen molecule and the complete set of manganese oxides, even though they are characterised by different oxidation states of the transition metal. The accuracy of the data in Table IV is very good when compared to recent reports (which have a mean error in the range of 7-17%) [25, 30]. This larger error can be attributed partially to the functionals used (PW91, PBE, PBE+U, PBE0 and HSE) and partially to the approaches adopted for the evaluation of μ^0_{Mn} and $\mu^0_{\mathrm{O}_2}$, which did not adequately account for limited error cancellation in the respective approximations to DFT. Careful consideration of error cancellation can lead to significant improvements, as has been demonstrated in previous work [63]. However errors have to be expected when μ^0_{Mn} and $\mu^0_{\mathrm{O}_2}$ are calculated by using the *ab initio* energy of the metal and the oxygen molecule indiscriminately with respect to the density functional.

C. Phase Diagram

Phase diagrams, constructed from the experimental and calculated Gibbs formation energies, are compared in Figure 2. The calculated bulk $LaMnO_3$ stability region is in good agreement with experiment. It is noted that in Figure 2 the stability region of $LaMnO_3$ is

affected by even a small percentage deviation from the experimental $\Delta_f G^0$ of $LaMnO_3$ and Mn_3O_4 (1% and 2.4%, respectively). However, from the previous studies [25, 30], the set of calculations with the lowest mean error had a 7% mean error with the largest deviation of 16% for MnO_2.

FIG. 2: Two-dimensional phase diagrams obtained by using the experimental and calculated Gibbs formation energy at standard conditions.

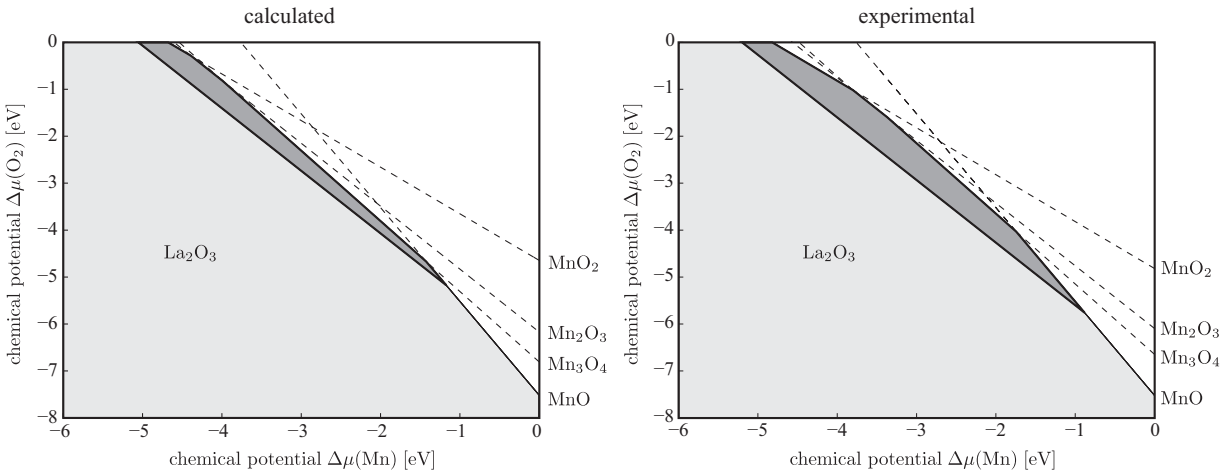

Figure 3 shows the phase diagram in 3D space by inclusion of the $\Delta\mu^0_{\mathrm{La}}$ axis. This allows for a better understanding of the stability of each compound and limiting phase equilibria. The decomposition of $LaMnO_3$ into La_2O_3 and gaseous oxygen sets the lower limit of the chemical potential of manganese. On the other hand, the upper limit for the manganese chemical potential varies strongly according to the environment. In strongly oxidising environments, the stability of $LaMnO_3$ is limited by the manganese oxide that can stabilise the most oxygen (MnO_2), while the reverse is true for a strongly reducing environment (Mn). Under midly redu cing or oxidizing conditions, $LaMnO_3$ forms equilibria with Mn_3O_4 and Mn_2O_3, which contain the intermediate (III) oxidation state of manganese.

Finally, the $LaMnO_3$ bulk stability region sets meaningful limits of the chemical potentials for the investigation of surface terminations, which is a prerequisite for the investigation of catalytic properties in relation to AFC applications.

FIG. 3: Three-dimensional phase diagram constructed from the calculated Gibbs formation energies at STP. Note that the $\Delta\mu_{O_2}$ axis is reversed with respect to plots in Figure 2. The stability region of $LaMnO_3$ is represented as the shaded area.

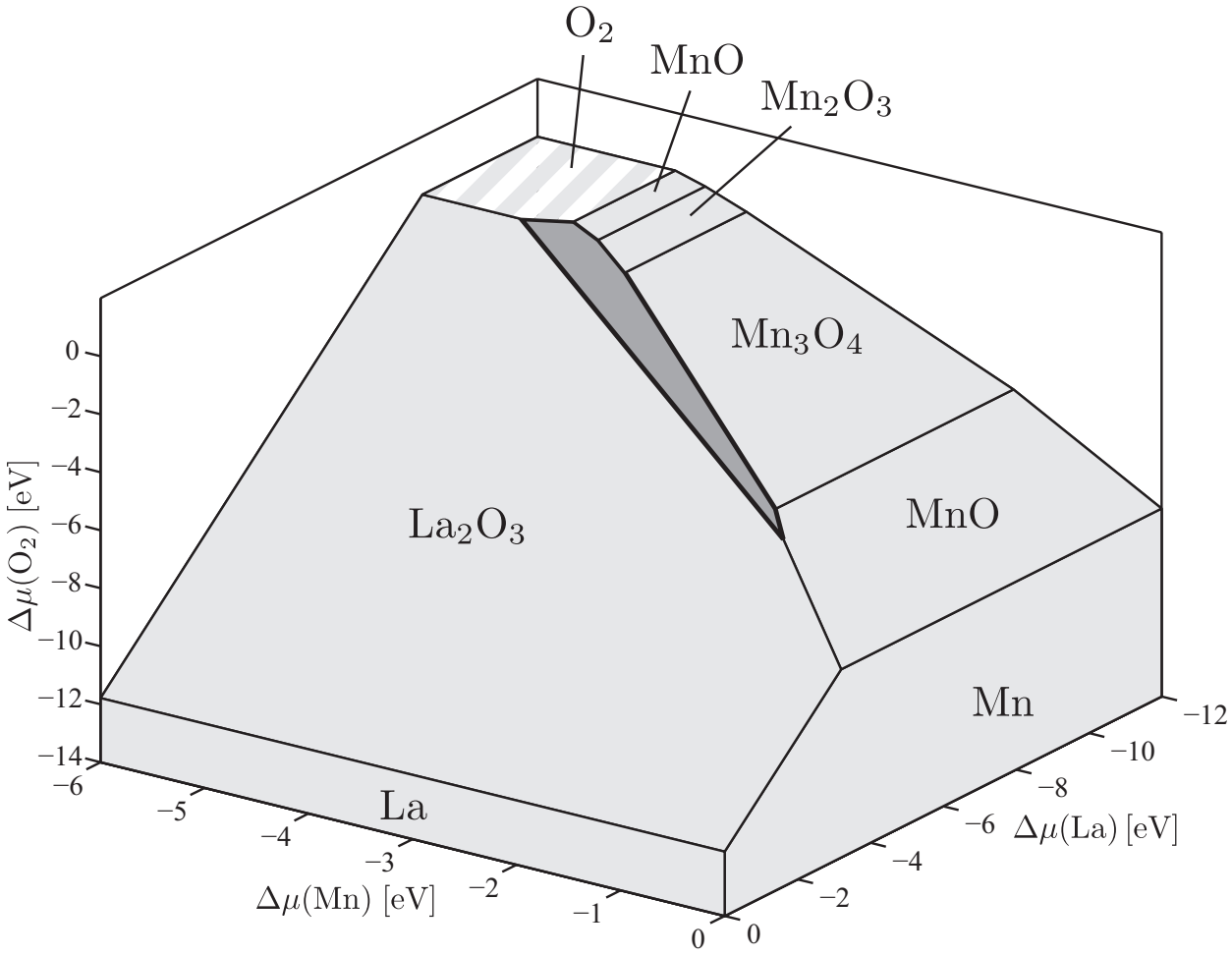

V. CONCLUSIONS

The thermodynamic phase stability of bulk $LaMnO_3$ and the manganese oxides have been investigated using hybrid DFT with periodic boundary conditions. The most stable geometric and magnetic phases of the compounds in the La-Mn-O system were determined and used to calculate the Gibbs formation energies. Quantitative agreement between calcualted and experimental formation energies at standard temperature and pressure was achieved (a mean error of 1.6%). This allowed to investigate the different phase equilibria that confine the stability region of bulk $LaMnO_3$ in chemical potential space, and therefore the region

where any surfaces of $LaMnO_3$ can be stable, for the complete system where metals, oxides, and gases partake.

The methodology developed was key to this investigation, as it allowed for the accurate calculation of the oxygen and manganese chemical potentials, and subsequently demonstrated that DFT simulations using the B3LYP functional can accurately predict the thermodynamics for the range of different valence states of the manganese oxides.

With regards to the study of the $LaMnO_3$ as a catalyst in AFCs, this is crucial, as the surfaces of $LaMnO_3$ are certain to contain multiple oxidation states of manganese. In conclusion, our methodology properly described the thermodynamics of bulk $LaMnO_3$ and will be able to address its surfaces.

Acknowledgments

This work made use of the high performance computing facilities of Imperial College London and - via membership of the UK's HPC Materials Chemistry Consortium funded by EPSRC (EP/F067496) - of HECToR, the UK's national high-performance computing service, which is provided by UoE HPCx Ltd at the University of Edinburgh, Cray Inc and NAG Ltd, and funded by the Office of Science and Technology through EPSRC's High End Computing Programme.

---

[1] S. Jin, T. H. Tiefel, M. McCormack, R. A. Fastnacht, R. Ramesh, and L. H. Chen, Science **264**, 413 (1994).

[2] S. Tao, J. Irvine, and J. Kilner, Advanced Materials **17**, 1734 (2005).

[3] T. Ishihara, *Perovskite Oxide for Solid Oxide Fuel Cells* (Springer, 2009).

[4] M. Hayashi, H. Uemura, K. Shimanoe, N. Miura, and N. Yamazoe, Journal of The Electrochemical Society **151**, A158 (2004), URL `http://link.aip.org/link/?JES/151/A158/1`.

[5] F. Bidault, D. Brett, P. Middleton, and N. Brandon, Journal of Power Sources **187**, 39 (2009), ISSN 0378-7753, URL `http://www.sciencedirect.com/science/article/B6TH1-4TVJ3M1-3/2/2c512ad07e9c63907bba295eed27a747`.

[6] J. A. M. V. Roosmalen, E. H. P. Cordfunke, R. B. Helmholdt, and H. W. Zand-

bergen, Journal of Solid State Chemistry **110**, 100 (1994), ISSN 0022-4596, URL http://www.sciencedirect.com/science/article/B6WM2-45P0GJW-1V/2/565a08f5e5dc2274033a41755f5e4151.

[7] P. Norby, I. G. K. Andersen, E. K. Andersen, and N. H. Andersen, Journal of Solid State Chemistry **119**, 191 (1995), ISSN 0022-4596, URL http://www.sciencedirect.com/science/article/B6WM2-471VJ1W-10/2/390dc4ecca79f3af77f9fcb3b0ee5ea3.

[8] H. Satoh, M. Takagi, K. ichi Kinukawa, and N. Kamegashira, Thermochimica Acta **299**, 123 (1997), ISSN 0040-6031, 14th IUPAC Conference on Chemical Thermodynamics, URL http://www.sciencedirect.com/science/article/B6THV-49CTJ51-K/2/5d0ddd8de32e4a8855e8f18e76fd4e0f.

[9] C. Oliva and L. Forni, Catalysis Communications **1**, 5 (2000), ISSN 1566-7367, URL http://www.sciencedirect.com/science/article/B6W7K-422G9TM-3/2/64de04aaf96be34a6b884c6adb23e662.

[10] D. S. JUNG, S. K. HONG, and Y. C. KANG, Journal of the Ceramic Society of Japan **116**, 141 (2008).

[11] Y. Shimizu and T. Murata, Journal of the American Ceramic Society **80**, 2702 (1997), ISSN 1551-2916, URL http://dx.doi.org/10.1111/j.1151-2916.1997.tb03178.x.

[12] J. Rodríguez-Carvajal, M. Hennion, F. Moussa, A. H. Moudden, L. Pinsard, and A. Revcolevschi, Phys. Rev. B **57**, R3189 (1998).

[13] K. Kitayama, Journal of Solid State Chemistry **153**, 336 (2000), ISSN 0022-4596.

[14] R. Singh, M. Malviya, Anindita, A. Sinha, and P. Chartier, Electrochimica Acta **52**, 4264 (2007), ISSN 0013-4686, URL http://www.sciencedirect.com/science/article/B6TG0-4MS9K42-2/2/6b2a4df5d19f66280e7d230d23c31058.

[15] Y.-S. Su, T. A. Kaplan, S. D. Mahanti, and J. F. Harrison, Phys. Rev. B **61**, 1324 (2000).

[16] M. Nicastro and C. H. Patterson, Phys. Rev. B **65**, 205111 (2002).

[17] D. Muñoz, N. M. Harrison, and F. Illas, Phys. Rev. B **69**, 085115 (2004).

[18] S. Piskunov, E. Spohr, T. Jacob, E. A. Kotomin, and D. E. Ellis, Phys. Rev. B **76**, 012410 (2007).

[19] R. A. Evarestov, E. A. Kotomin, D. Fuks, J. Felsteiner, and J. Maier, Applied Surface Science **238**, 457 (2004), ISSN 0169-4332, aPHYS'03 Special Issue, URL http://www.sciencedirect.com/science/article/B6THY-4CYPXP3-6/2/

93ca7aeb19021546e3141c37beaf52a9.

[20] S. Piskunov, E. Heifets, T. Jacob, E. A. Kotomin, D. E. Ellis, and E. Spohr, Phys. Rev. B **78**, 121406 (2008).

[21] Y. Choi, D. S. Mebane, M. C. Lin, and M. Liu, Chemistry of Materials **19**, 1690 (2007), http://pubs.acs.org/doi/pdf/10.1021/cm062616e, URL http://pubs.acs.org/doi/abs/10.1021/cm062616e.

[22] E. A. Kotomin, Y. Mastrikov, E. Heifets, and J. Maier, Phys. Chem. Chem. Phys. **10**, 4644 (2008).

[23] Y. Choi, M. E. Lynch, M. C. Lin, and M. Liu, The Journal of Physical Chemistry C **113**, 7290 (2009), http://pubs.acs.org/doi/pdf/10.1021/jp811021p, URL http://pubs.acs.org/doi/abs/10.1021/jp811021p.

[24] E. A. Kotomin, R. A. Evarestov, Y. A. Mastrikov, and J. Maier, Phys. Chem. Chem. Phys. **7**, 2346 (2005), URL http://dx.doi.org/10.1039/B503272E.

[25] Y. Mastrikov, E. Heifets, E. Kotomin, and J. Maier, Surface Science **603**, 326 (2009), ISSN 0039-6028, URL http://www.sciencedirect.com/science/article/B6TVX-4V3HF6X-3/2/8845773383efa7705d76a804a9dbf013.

[26] L. B. Pankratz, U. S. Bureau of Mines Bulletin **672**, 509 (1982).

[27] R. A. Robie and B. S. Hemingway, The Journal of Chemical Thermodynamics **17**, 165 (1985), ISSN 0021-9614, URL http://www.sciencedirect.com/science/article/B6WHM-4CRHCDW-10J/2/0cf9e7c990cabb14b8b3033e0b6d334c.

[28] A. N. Sophie Fritsch, Journal of the American Ceramic Society **79**, 1761 (1996).

[29] R. Amankwah and C. Pickles, Journal of Thermal Analysis and Calorimetry **98**, 849 (2009), ISSN 1388-6150, 10.1007/s10973-009-0273-3, URL http://dx.doi.org/10.1007/s10973-009-0273-3.

[30] C. Franchini, R. Podloucky, J. Paier, M. Marsman, and G. Kresse, Phys. Rev. B **75**, 195128 (2007).

[31] J. Muscat, A. Wander, and N. Harrison, Chemical Physics Letters **342**, 397 (2001), ISSN 0009-2614, URL http://www.sciencedirect.com/science/article/B6TFN-43F67HJ-T/2/1ee4aafa1605a010e41f04345e3a3d10.

[32] F. Cor, M. Alfredsson, G. Mallia, D. S. Middlemiss, W. C. Mackrodt, R. Dovesi, and R. Orlando, **113**, 171 (2004), 10.1007/b97944, URL http://dx.doi.org/10.1007/b97944.

[33] L. M. Liborio, C. L. Bailey, G. Mallia, S. Tomic, and N. M. Harrison, Journal of Applied Physics **109**, 023519 (pages 9) (2011), URL http://link.aip.org/link/?JAP/109/023519/1.

[34] K. Johnston, M. R. Castell, A. T. Paxton, and M. W. Finnis, Phys. Rev. B **70**, 085415 (2004).

[35] *http://webbook.nist.gov/chemistry/* (????).

[36] CRC, *Handbook of Chemistry & Physics 91st Edition* (Taylor and Francis Group, 2010).

[37] D. Kramer and G. Ceder, Chemistry of Materials **21**, 3799 (2009), http://pubs.acs.org/doi/pdf/10.1021/cm9008943, URL http://pubs.acs.org/doi/abs/10.1021/cm9008943.

[38] R. Dovesi, V. R. Saunders, C. Roetti, R. Orlando, C. M. Zicovich-Wilson, F. Pascale, B. Civalleri, K. Doll, N. M. Harrison, I. J. Bush, et al., CRYSTAL09 *User's Manual*, Università di Torino (Torino, 2010).

[39] *http://www.crystal.unito.it/Basis_Sets/Ptable.html* (????).

[40] C. Pisani, R. Dovesi, and C. Roetti, *Hartree-Fock ab initio Treatment of Crystalline Systems*, vol. 48 of *Lecture Notes in Chemistry* (Springer Verlag, Heidelberg, 1988).

[41] E. O. Wollan and W. C. Koehler, Phys. Rev. **100**, 545 (1955).

[42] *http://cds.dl.ac.uk/icsd/* (????).

[43] B. C. Hauback, H. Fjellvg, and N. Sakai, Journal of Solid State Chemistry **124**, 43 (1996), ISSN 0022-4596, URL http://www.sciencedirect.com/science/article/B6WM2-45PVM14-2P/2/df5c2b8796897a24828a11e626576efd.

[44] N. Hirosaki, S. Ogata, and C. Kocer, Journal of Alloys and Compounds **351**, 31 (2003), ISSN 0925-8388, URL http://www.sciencedirect.com/science/article/B6TWY-47HC558-5/2/d904ca808c39990365f9d13c7e27d899.

[45] J. E. Post and P. J. Heaney, American Mineralogist **89**, 969 (2004), http://ammin.geoscienceworld.org/cgi/reprint/89/7/969.pdf, URL http://ammin.geoscienceworld.org/cgi/content/abstract/89/7/969.

[46] S. Geller, Acta Crystallographica Section B **27**, 821 (1971), URL http://dx.doi.org/10.1107/S0567740871002966.

[47] V. Baron, J. Gutzmer, H. Rundlof, and R. Tellgren, American Mineralogist **83**, 786 (1998), http://ammin.geoscienceworld.org/cgi/reprint/83/7-8/786.pdf, URL http://ammin.geoscienceworld.org/cgi/content/abstract/83/7-8/786.

[48] D. Taylor, Transactions and Journal of the British Ceramic Society **83**, 5 (1984).

[49] A. Bolzan, C. Fong, B. Kennedy, and C. Howard, Australian Journal of Chemistry **46**, 939 (1993).

[50] X.-F. Wang, Q.-X. Li, X.-Y. Chu, and F. S-H., Chemical Journal of Chinese Universities **28**, 821 (2007).

[51] C. R. Ross, D. C. Rubie, and E. Paris, American Mineralogist **75**, 1249 (1990), URL `http://ammin.geoscienceworld.org/cgi/content/abstract/75/11-12/1249`.

[52] V. Dyakonov, F. N. Bukhanko, V. I. Kamenev, E. E. Zubov, M. Arciszewska, W. Dobrowolski, V. Mikhaylov, R. Puźniak, A. Wiśniewski, K. Piotrowski, et al., Phys. Rev. B **77**, 214428 (2008).

[53] M. Mikami and S. Nakamura, Journal of Alloys and Compounds **408-412**, 687 (2006), ISSN 0925-8388, URL `http://www.sciencedirect.com/science/article/B6TWY-4GJVB3R-2/2/e1c112487b34390d37fe8895da0d947f`.

[54] P. R. B. Shirley Turner, Nature **304**, 143 (1983).

[55] D. Balachandran, D. Morgan, G. Ceder, and A. van de Walle, Journal of Solid State Chemistry **173**, 462 (2003), ISSN 0022-4596, URL `http://www.sciencedirect.com/science/article/B6WM2-4938KV9-Y/2/cad198826a1cbdc7e5ff621f0bacfbd1`.

[56] M. Regulski, R. Przenioslo, I. Sosnowska, D. Hohlwein, and R. Schneider, Journal of Alloys and Compounds **362**, 236 (2004), ISSN 0925-8388, URL `http://www.sciencedirect.com/science/article/B6TWY-497RGT8-3/2/64fbe71c68da1d58e1205791ce7cda15`.

[57] S. Mukherjee, A. K. Pal, S. Bhattacharya, and J. Raittila, Phys. Rev. B **74**, 104413 (2006).

[58] T. Suzuki and T. Katsufuji, Journal of Physics: Conference Series **150**, 042195 (2009), URL `http://stacks.iop.org/1742-6596/150/i=4/a=042195`.

[59] R. Tackett, G. Lawes, B. C. Melot, M. Grossman, E. S. Toberer, and R. Seshadri, Phys. Rev. B **76**, 024409 (2007).

[60] W. L. Roth, Phys. Rev. **110**, 1333 (1958).

[61] H. Shaked, J. Faber, and R. L. Hitterman, Phys. Rev. B **38**, 11901 (1988).

[62] M. D. Towler, N. L. Allan, N. M. Harrison, V. R. Saunders, W. C. Mackrodt, and E. Aprà, Phys. Rev. B **50**, 5041 (1994).

[63] L. Wang, T. Maxisch, and G. Ceder, Phys. Rev. B **73**, 195107 (2006).

[64] K. T. Jacob and M. Attaluri, J. Mater. Chem. **13**, 934 (2003).